fire

MDPI

Article

Sediment Response after Wildfires in Mountain Streams and Their Effects on Cultural Heritage: The Case of the 2021 Navalacruz Wildfire (Avila, Spain)

Jose A. Ortega-Becerril [1,*], Clara Suarez [1], Daniel Vázquez-Tarrío [2], Julio Garrote [3,*] and Miguel Gomez-Heras [1]

[1] Geology and Geochemistry Department, Sciences Faculty, Universidad Autónoma de Madrid, 28049 Madrid, Spain; clara.suarezr@estudiante.uam.es (C.S.); miguel.gomezheras@uam.es (M.G.-H.)
[2] Department of Geo-Hazards & Climate Change, Geological and Mining Institute of Spain (IGME), Spanish National Research Council (CSIC), 28003 Madrid, Spain; d.vazqueztarrio@igme.es
[3] Geodynamics, Stratigraphy and Palaeontology Department, Universidad Complutense de Madrid, 28040 Madrid, Spain
* Correspondence: j.ortega@uam.es (J.A.O.-B.); juliog@ucm.es (J.G.)

Abstract: The 2021 Navalacruz wildfire occurred in a mountainous area in the Sistema Central (Spain). Despite having an average low severity index (dNBR), the loss of vegetation cover associated with the fire was responsible for a high rate of sedimentation in the rivers and streams. Additionally, the burned area affected up to 60 cultural heritage sites, including archaeological and ethnological sites, and damage ranged from burnt pieces of wood to the burial of archaeological sites. In the present work, we document and analyze the post-fire evolution in several rivers and streams. This is based on a field survey of infiltration rates, hydrodynamic modeling, and the study of channel morphological changes. Our analysis revealed how the first post-fire rains caused the mobilization and transport of ashes. This created hydrophobicity in the soils, resulting in large amounts of materials being transported to rivers and streams by subsequent medium- and low-magnitude storms. A hydrological and hydraulic model of the study catchments under pre- and post-fire conditions suggests that these trends are a consequence of a post-fire increase in flow rates for similar rainfall scenarios. In this respect, our estimates point at a significant increase in sediment transport capacities associated with this post-fire increase in flow rates. The combination of locally steep slopes with high-severity fire patches, and a considerable regolith (derived from pre-fire weathering), resulted in a series of cascading responses, such as an exacerbated supply of sand to the drainage network and the triggering of debris flows, followed by erosion and entrenchment.

Keywords: wildfires; sediment yield; hydrophobicity; curve number; erosion; rock weathering; floods; cultural heritage; river morphology; debris flow

check for updates

Citation: Ortega-Becerril, J.A.; Suarez, C.; Vázquez-Tarrío, D.; Garrote, J.; Gomez-Heras, M. Sediment Response after Wildfires in Mountain Streams and Their Effects on Cultural Heritage: The Case of the 2021 Navalacruz Wildfire (Avila, Spain). *Fire* **2024**, *7*, 52. https://doi.org/10.3390/fire7020052

Academic Editor: Scott Mooney

Received: 13 December 2023
Revised: 1 February 2024
Accepted: 5 February 2024
Published: 8 February 2024

Copyright: © 2024 by the authors. Licensee MDPI, Basel, Switzerland. This article is an open access article distributed under the terms and conditions of the Creative Commons Attribution (CC BY) license (https://creativecommons.org/licenses/by/4.0/).

1. Introduction

Wildfires represent a critical natural phenomenon that can have far-reaching impacts on various ecosystems and environmental processes, in addition to causing damage to human structures and cultural heritage sites. Beyond the immediate devastation that they cause to landscapes, wildfires can also lead to significant alterations in sediment transport patterns and subsequently induce changes in river morphology. Understanding the complex relationships between wildfire, sediment transport dynamics, and river morphology is essential to predicting and mitigating the long-term effects of these events on both natural habitats and human structures.

Wildfires are a fundamental biophysical driver of, firstly, rock weathering and soil erosion and, secondly, post-fire colluvial–fluvial sediment transport in Mediterranean environments. The dispersal of sediment through catchments from the source to sink [1]

triggers morphological changes in channels and valley floors [2]. These changes in rivers are due to high sediment yields because the channel becomes unstable [3], as well as in hillslopes, where post-fire soil with low cohesion can be susceptible to the net downhill sediment transport of soil by rain splash [4]. However, these changes are not necessarily triggered by high-magnitude events [3,5,6]. Channel instability can also occur with low peak flows and without large, external increases in sediment supply. The progressive shift in channel morphology during the early stages, from plane bed (sediment accumulation) to riffle–pool morphologies, has been described by Ref. [3] as a response to floodplain occupation. In subsequent stages, extensive bank erosion leads to a dramatic change in channel morphology; this pattern has already been described by Ref. [7] and is related to transport-limited conditions resulting in channel deposition in the first storm and, subsequently, sediment-limited conditions leading to stream scouring and considerable downstream sediment transport.

Moreover, fire activity is one of the most significant drivers of aquatic degradation through surface runoff and ashes [8], and it triggers cascading effects over a wide range of spatiotemporal scales [9,10]. For instance, several authors have reported episodes of intense surface runoff occurring immediately after fires [5,11,12]. Although the documented time scale is imprecise, ranging from a few weeks/months up to two/three years after the event [11–14], fire clearly affects landscapes in the long term [15].

Wildfires are responsible for exacerbated sediment delivery to the drainage network of headwater streams. In this regard, the main suggested drivers of post-fire sediment production are fire severity, bare soil, rainfall characteristics (type, erosivity, and intensity), and hydrophobicity [12,16,17]. Fire-severe years can account for up to 90% of the total annual soil loss, and this is particularly problematic with the co-occurrence of high-intensity wildfires and post-fire floods [18]. In this respect, post-fire convective storms have been suggested to be responsible for 90% of the sediment generated [16], but due to the variable coverage of storms, the sediment response and degree of channel change can vary from little or negligible changes to extensive incision and aggradation [12].

The combination of severe wildfires and storms increases long-term suspended sediment fluxes [19] and the occurrence of debris flows associated with convective storms with a low duration (<3 h) and a high intensity, with recurrence intervals of two years or less [5]. Conversely, Ref. [20] noted that post-fire debris flows occur mostly in response to moderate-to-severe rainfall. They identified slopes steeper than 30% as particularly susceptible to soil erosion. Furthermore, vegetation dams, when burned during wildfires, can rapidly release large amounts of sediment into river channels and trigger debris flows [15,21]. As a result of all the above processes, post-fire sediment yields from debris flows have been reported to be 2–3 orders of magnitude greater than under normal, non-burned conditions [6].

In addition, all the above processes represent a risk to human structures and properties, with cultural heritage sites being of particular interest, as their damage or destruction represents a loss that goes beyond the material loss. Archaeological, vernacular, and small-scale heritage buildings and structures in rural areas are particularly at risk, as they are often located in secluded areas without proper protection measurements and reduced access for firefighters [22,23].

Fire affects stonemade heritage structures, generating primary and secondary damage [24]. Primary damage may include that caused directly by high temperatures, which can reach up to 1000 °C during a fire. Quartz-bearing rocks, such as granitic lithologies, exhibit intense spalling and granular disaggregation above 573 °C due to quartz-phase transitions that involve an intense volume change [25–27]. Furthermore, as primary damage, ion-rich ashes and fumes may penetrate the porous system of rocks and lead, in turn, to secondary damage caused by the formation of soluble salts which contribute to increasing long-term weathering [28]. Both processes weaken the rock structure, which may lead to the destruction of stonemade cultural structures. Subsequent floods accompanied by exacerbated sediment delivery may obliterate some structures, causing secondary damage.

A case in point of this last process in the studied area is the destruction of the centennial "Puente de Muñico" (Muñico Bridge) due to the floods caused after the wildfire [29].

In this paper, we studied the effects of the fourth historical wildfire ever recorded in the Sierra de Paramera (Avila, Spain). This fire event was called the Navalacruz fire because it started from a roadside crash in the municipality of Navalacruz. The area affected by the fire has a remarkable cultural heritage, a low population, and a well-preserved landscape. In total, 46 out of the 60 inventoried cultural assets in the area affected by the fire were damaged during the fire or just after the fire because of floods and sediment transport. Besides the destruction of the above-mentioned Muñico Bridge, 10 of these assets experienced severe damage, and only nine out of the sixty inventoried assets did not suffer any damage as a consequence of the fire [29].

We explore the meteorological thresholds through which this wildfire influenced sediment mobilization and transport, as well as how these transported sediments reshaped river channels and floodplains. Our objectives are the following: (1) to establish the basin's hydro-sedimentary response to low-intensity and high-frequency rainfall events; (2) to determine whether the previous state of weathering in the soils across the watershed may be able to enhance the river's response to wildfire; (3) to determine the degree of influence of hydrophobicity on flood hydrographs after the wildfire; (4) to estimate the sediment volume transported during the early stages after the wildfire and to compare direct in-field measurements with indirect 2D hydrodynamic results; and (5) to determine the degree of damage to cultural heritage sites, either by direct causes, such as the fire itself, or by indirect causes, such as subsequent flooding. Despite the short observation period (~2 years after the fire), this study has already allowed us to highlight important aspects of the hydro-sedimentary response of the study catchments to the fire.

2. Study Area and Navalacruz Wildfire

The Sierra de la Paramera is a mountain range situated in the northeastern region of the Spanish Central System (Figure 1). It displays a distinct asymmetry, characterized by a steep slope on its southern side and a gentle slope on its northern side. The total rainfall amount is 400 mm in the northern side and 700 mm in the southern side. This is related to the asymmetry of the mountain range. The rainy season corresponds to late autumn (November–December), with snowmelt in early spring, and the dry season occurs during summer with high temperatures. Records show that, in a return period of 3 years, the rainfall exceeded 250 mm in the span of 1 week [30].

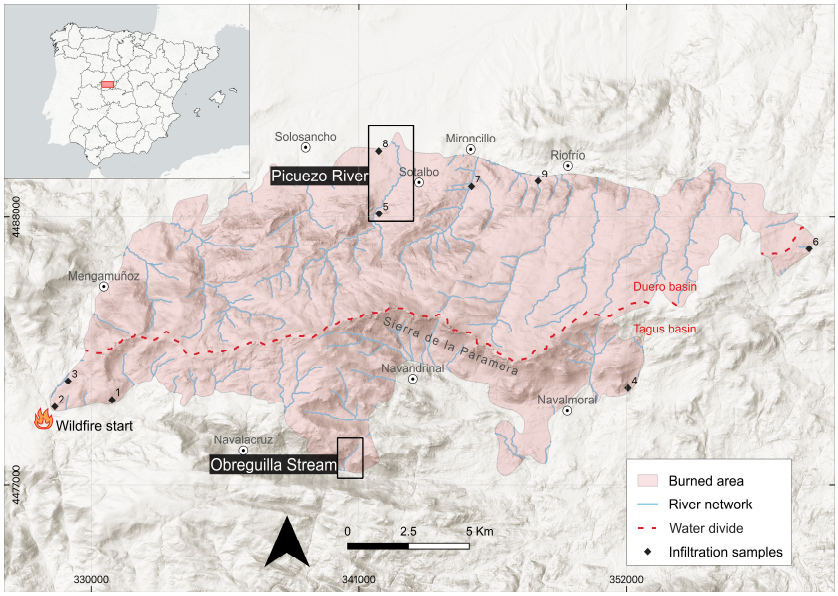


Figure 1. Location of the study area, wildfire perimeter, studied catchments (in boxes), and infiltration test sites (black dots).

The Sierra de la Paramera corresponds to an uplifted asymmetric granitic block within the pop-up and pop-down structure that originated during the Alpine orogeny (Miocene) which constitutes the central portion of the Central System. The coarse-grained granite forming this relief weathers, leaving a regolith formed mainly by sand and gravel, so-called grus [31]. The grus displays a shear strength resembling that of coarse sand [32], and when the grus is not stabilized by vegetation, it becomes an important source of sediments through runoff, particularly in the areas with higher slope (Figure S1).

The mountain range acts as a watershed divide between the Tagus to the south and the Duero basin to the north. The peaks reach 2100 m and are dissected by deep valleys. The main rivers are the Picuezo–Adaja Rivers in the north and the Navalacruz–Alberche Rivers in the south. Due to their steep slopes, most of the channels on the southern side are ephemeral mountain streams that flow directly toward the main valleys. The geology of the study area (Figure S2) is mainly composed of the following: (1) coarse-grained biotite granites; (2) granitic porphyry dikes, which predominate in areas with slopes of 20–30%; and (3) slope deposits (colluvium) composed of cobbles and silt. In the valleys, (4) coarse and fine fluvial deposits predominate.

The joint network of the granitic bedrock conditions heterogeneous weathering which leaves relatively unweathered boulders embedded within a weathered mantle of variable thickness. Granite weathering occurs mainly due to hydrolysis, and weathering rates depend directly on precipitation and temperature [33]. Felsic Fe-poor rocks, such as this granite, favor the formation of a thick regolith when the climatic conditions are appropriate [34]. However, grus' thickness depends ultimately on erosion rates, as denudation limits weathering advance [35].

In the studied area, the grus' thickness is variable, and it is generally thin, particularly in the steepest sloping south flank of the Sierra, where it is between 1 m [36] and 3–4 m, but it can attain deeper soils in certain areas of the southern flank [30], in comparison to the tens of meters in the northern flank [37]. The lack of sediment on the southern side is due to the more powerful erosion of the Alberche River, which has greater slopes and a greater erosive capacity than the Adaja River. On the northern side, the grus is an important source of sediment that migrates through the riverbeds when the vegetation is removed.

The vegetation in the area is divided into Mountain *Cytisus* formations, mountain pastures, sparse forest patches of sclerophyllous oak and junipers, and patches of coniferous forest (Figure 2). The central area is devoid of vegetation, with granitic outcrops.

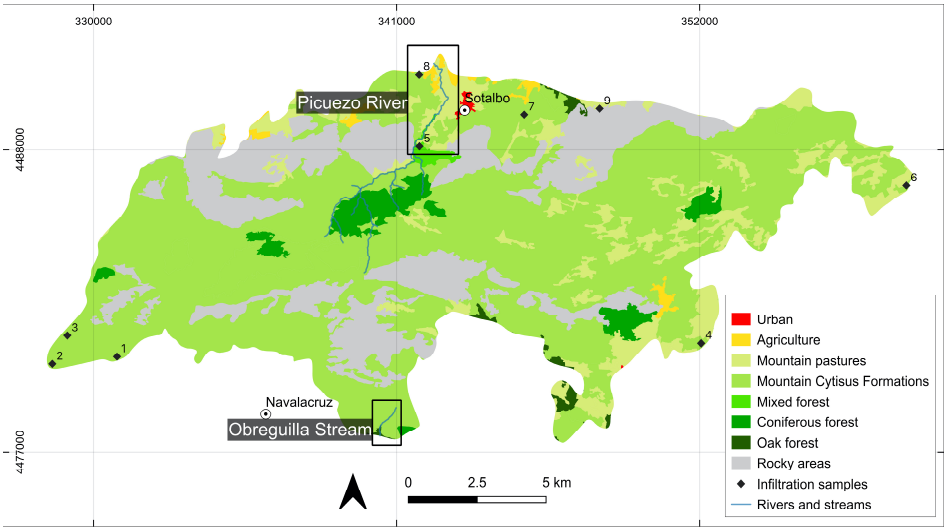


Figure 2. Land use map of burned area showing mostly mountain pastures, Mountain *Cytisus* formations, and sparse areas of coniferous and oak forest. Black dots show the infiltration test sites and black boxes show the studied catchments.

The Navalacruz wildfire, which burned 22,000 ha, was the fourth most serious fire in extent in Spain since records began (Figure 1). The fire started on 14 August 2021 as a result of a vehicular accident on a road; the fire then spread rapidly through a mountainous area due to wind speed and was stabilized after two days. It was finally brought under control on 17 August. In the days preceding the fire, Copernicus [38] warned of favorable meteorological conditions for a wildfire; the Fire Weather Index (FWI) was higher, as well as the BUI index (total amount of fuel available for combustion). The SW–NE wind direction affected the Sierra de la Paramera, a sparsely populated area, resulting in no fatalities. Despite the low mean intensity (Figure 3), a large area was burnt, as the fire spread over very rugged terrain consisting of granitic outcrops, high pastures, and scrubland, which made it difficult to extinguish with land-based means.

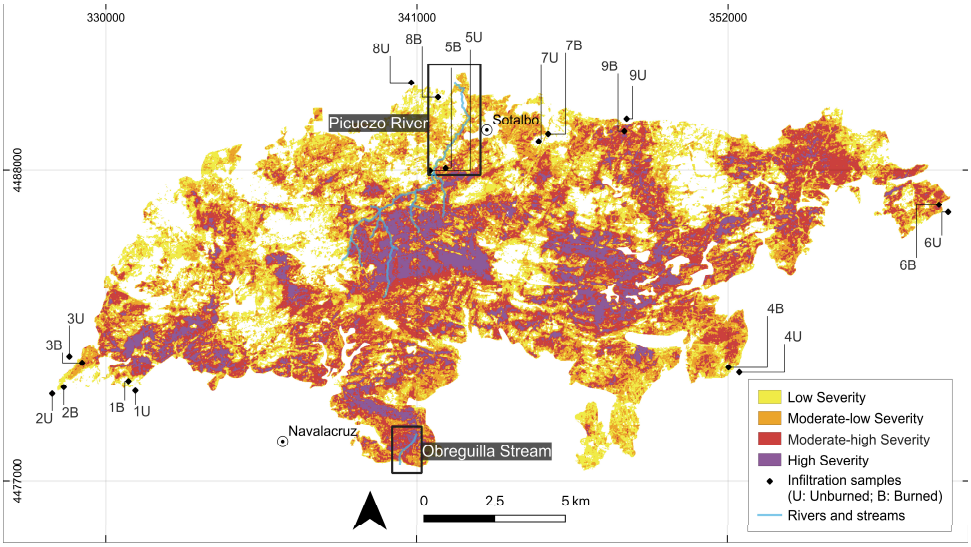


Figure 3. dNBR index of the studied area of Navalacruz. Black dots show the infiltration test sites and black boxes show the studied catchments.

3. Materials and Methods

Sentinel-2 was used as the remote sensing platform (corrected with Sen2Cor v2.10), with images from before and after each fire used for the delimitation of the fire's extent and severity and for calculating the dNBR index, following the classification used by the United States Geological Survey [39].

The degree of influence of the wildfire on soil infiltration was assessed using a randomized systematic design in two different areas: burned and unburned areas. Nine infiltration sites were selected. At each site, at least 2 to 4 infiltration tests were conducted using the single ring method [40]. Sites were selected according to the type of vegetation cover. The sites were chosen to be more representative of the main vegetation types: mountain pastures, Mountain *Cytisus* formations, and patches of coniferous and oak trees. Due to the homogeneous geology of the area, most of the soils are granitic regolith with thicknesses ranging from 1 m on the southern side to 10 m on the northern side. We measured all samples in flat areas.

Precipitation data were obtained from the Spanish state meteorological agency (AEMET). We used the station closest to the area (Avila station 4222, 12 km from the fire). In order to obtain the best information about the rainfall distribution during the events, we used radar information from AEMET with 10 min time intervals.

A two-dimensional (2D) hydrodynamic model, Iber software v3.3 [41], was used to reconstruct the rainfall events. Iber is a 2D numerical model that simulates free surface flow in rivers by solving the 2D Saint-Venant equations. To determine the flow depth and the two components of the depth-averaged velocity in the XY plane, Iber software

solves the full depth-averaged shallow water equations. These equations are solved using unstructured meshes and explicit finite volume techniques.

The Iber software simulations were based on a 5 m resolution DEM, freely available from the Spanish National Geographic Institute (IGN), derived from LiDAR data. The simulation used rainfall data (AEMET) from meteorological radar sensors as water inputs to the two different basins considered here. Other parameters included in the hydrodynamic simulations were the Soil Conservation Service–Curve Number (SCS-CN) as the rainfall loss and the surface roughness coefficient (Manning's value). The last two variables were considered for both the pre-fire and post-fire scenarios.

The use of the SCS-CN loss method is well developed and widely accepted in the USA and other countries (e.g., [42–44]). The SCS-CN values were derived from the CORINE Land Cover (CLC) data and the proposed values for each CLC unit in the Spanish guide [45]. The assignment of SCS-CN values for post-fire conditions used the recommendations of the aforementioned Spanish guide, as well as the suggestions of Refs. [46,47], considering a moderate soil burn severity.

The surface roughness coefficient (Manning's value) for the pre-fire conditions was set according to the suggestion by Ref. [48]. For post-fire conditions, the previous (pre-fire) values were reduced to 40% of their original value, following the recommendations of Refs. [49,50]. However, the previously suggested reduction in Manning's value was not applied to the entire study area, as the bare rock outcrops were not affected by vegetation changes due to the fire occurrence; therefore, Manning's values were not changed for the rock outcrop areas or the channels (whose surface roughness is much more related to the distribution of gravel, pebbles, or boulders than to vegetative effects).

From the available pre- and post-fire hydrodynamic model results, the discharge hydrograph and shear stress (τ) values were used to define the hydrological behavior and changes due to the Navalacruz 2021 wildfire. The analysis focused on two different basins: the small basin of the Obreguilla Creek (with only 4 km^2) and the medium basin of the Picuezo River (with an area of 25 km^2).

In order to detect changes in fluvial streams, we identified 38 checkpoints, from which we finally selected 14 sites with the criteria of being easily accessible from the roads and open to being allowed to take photographs, where a time series of images could be used to compare the degree of evolution: basically unchanged, predominantly sedimentation, and predominantly erosion. The first series of images was taken a few days immediately after the fire and could therefore be considered the original starting framework prior to the river floods post-fire.

To study the post-fire sediment response in detail, we selected two catchments (see Figure 1): Obreguilla Creek, an ephemeral mountain stream located on the southern side, and the Picuezo River, a perennial stream and one of the main streams of the burned area. At both sites, we recorded the sediment extent (in planform and thickness) of the sediment wave that propagated downstream during the post-fire events. All length (sediment width and depth) and slope measurements were made using a TruPulse 360 R Laser Rangefinder. For the sediment contour in bars (the Picuezo River) and the fan perimeter at Obreguilla Creek, we used drone imagery and GPS. Sediment volumes were calculated from isopach maps.

To complement the field measurements, a two-step estimation of the effect of the fire on bedload mobilization rates was carried out. First, we tried to quantify the increase in sediment transport capacities that the fire might have caused compared to pre-fire conditions. To do this, we used the bedload formula developed in [51,52], which is an equation that performs reasonably well in mountain streams. According to this equation, the bedload transport rates (q_s) are proportional to

$$q_s \propto \frac{\tau^{*2.5}}{\left(1 + \frac{\tau_m^*}{\tau^*}\right)^4} \quad (1)$$

where τ^* is the dimensionless shear stress, which can be estimated as

$$\tau^* = \frac{\tau}{1650gD} \quad (2)$$

where τ is the shear stress and D is the particle size representative of the riverbed (the 84th percentile, according to Ref. [51]. Finally, $\tau_m{}^*$ is a model parameter, which can be obtained from the following expression:

$$\tau_m^* = 1.5S^{0.75} \quad (3)$$

By rearranging Equation (1), we arrived at the following expression:

$$\frac{q_{s_{postfire}}}{q_{s_{prefire}}} = \left(\frac{\tau_{post}}{\tau_{pre}}\right)^{6.5}\left(\frac{\tau_{pre}+\tau_m}{\tau_{post}+\tau_m}\right)^4\left(\frac{D_{pre}}{D_{post}}\right)^4 \quad (4)$$

The 2D hydrodynamical model allowed us to estimate the change in the shear stress distribution in the pre- and post-fire conditions. Then, we combined the hydrodynamical model outcomes with Equation (4) to estimate the average change in bedload transport capacities associated with the change in runoff volumes and flow rates induced by the wildfire. One unknown that precluded the complete application of Equation (4) was the uncertainty in the change in the grain size of the streambed linked to the wildfire, which was difficult to evaluate. Therefore, we decided to assume that there was no significant change in the grain size of the channel bed before and after the wildfire.

In the second step, we estimated the amount of bedload that was remobilized during the 2021 post-fire storm. To do this, we used a simple formula that is commonly used by engineers working on Alpine torrents with a "pulsating" bedload and high sediment concentrations. These conditions are probably not very different to those that prevailed in the Obreguilla and Picuezo Rivers (according to our field observations). This equation makes the sediment concentration (C) dependent on the square of the bed slope (S) [53]:

$$C = \beta \cdot S^2 \quad (5)$$

where β is an empirical coefficient for which different values have been proposed, e.g., 5.5 and 2.5, Chezy's roughness coefficient [53,54]. Recently, Ref. [53] found that this equation well describes the behavior of sediment pulses observed in channel experiments with a high sediment concentration, with an optimal value of β ~5. We applied Equation (5) to the modeled flow hydrogram of the storm for the Obreguilla and Picuezo Rivers. We tested three different values for β: 2, 5, and 8.

We used the range of damage of cultural assets after the wildfire published by Ref. [29]: no damage (0), slight (1), moderate (2), severe (3), or ruin/collapse (4). In addition, we carried out an on-the-spot comparison to make a visual assessment of most of the cultural assets and all of those affected by the floods.

4. Results

As reported in other lithologies [55,56], wildfires increase debris slope destabilization in the short term, as well as accelerating weathering rates in the medium and long terms, therefore accelerating the formation of new regolith. In the case of granites, this is exacerbated by temperature-induced cracking, particularly when fire exceeds 573 °C and the α–β quartz phase transition takes place [26]. Fire also removes vegetative cover (Figure 4). The grus displays a shear strength resembling that of coarse sand [32], and when grus is not stabilized by vegetation, it becomes an important source of sediments through runoff, particularly in areas with steeper slopes (Figure S1).

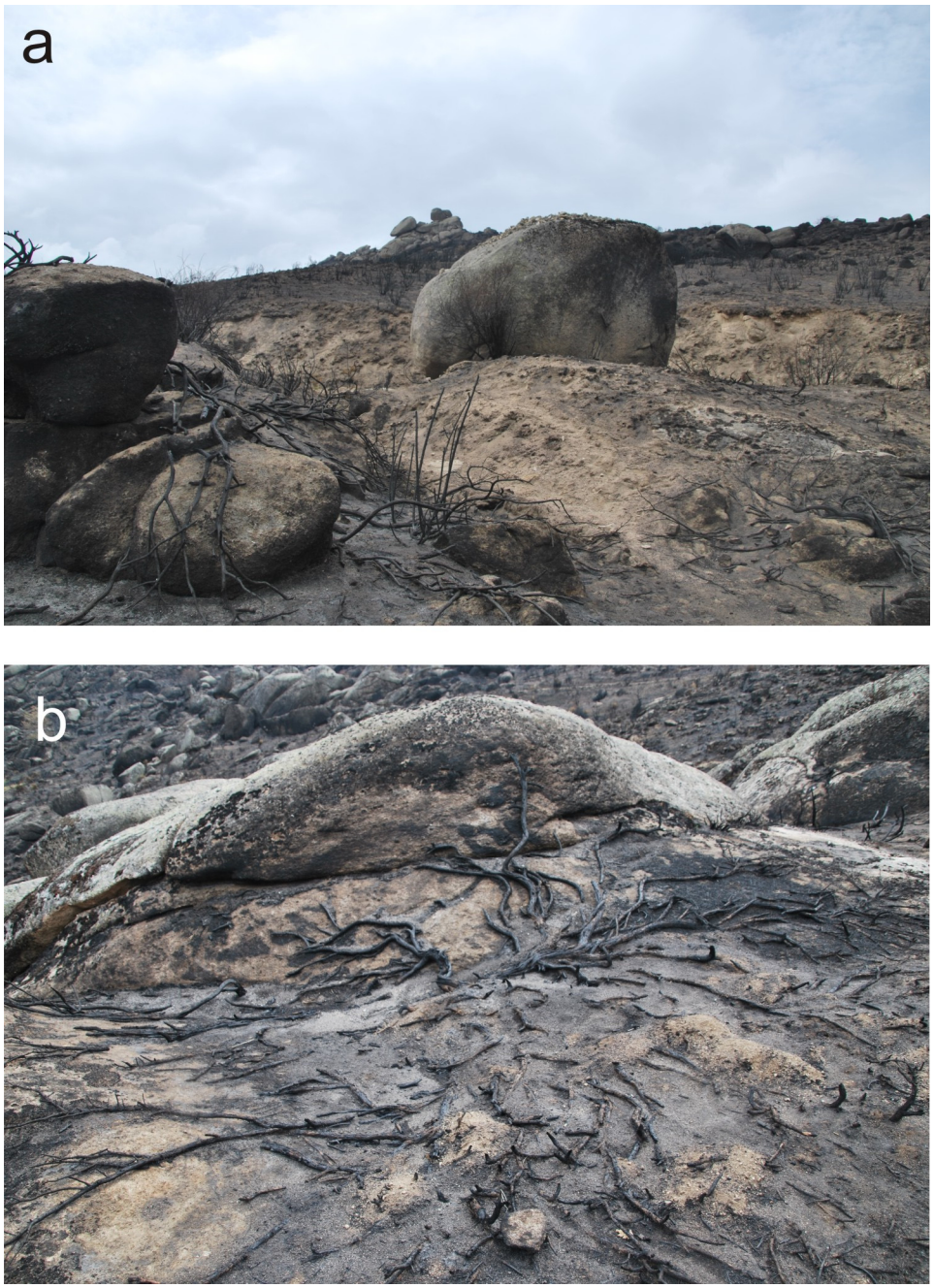


Figure 4. The main source of sediment on slopes and rivers comes from weathered granitic outcrops. (**a**) Exposed regolith on the northern side in Picuezo watershed. (**b**) Wide surface covered by Mountain *Cytisus* formations and the loss of protection for regolith soil after the wildfire. These pictures were taken on 13 September 2021, 27 days after the fire.

4.1. Post-Wildfire Rainfall Events

The wildfire occurred at the end of summer, just before the start of the rainy season. The results allowed us to identify three main groups of storms (G1, G2, and G3). In G1, we recognized four events immediately after the fire (events 1 to 4). The first event occurred 15 days after the end of the fire. As can be seen in Figure 5, the first four events showed moderate rainfall that did not exceed 32 mm but still caused significant changes in the rivers, with ash transport occurring first and then sand and mud transport occurring later. The event of 23–24 September was the largest of the four events (58.2 mm/cumulative rainfall), and it was considered of moderate–low magnitude. These rains caused the flooding of Garganta Obreguilla (with debris flow generation) and the Picuezo River. Other rainfall

events during the first two months after the fire were of low magnitude, but they still mobilized sediment along the channels.

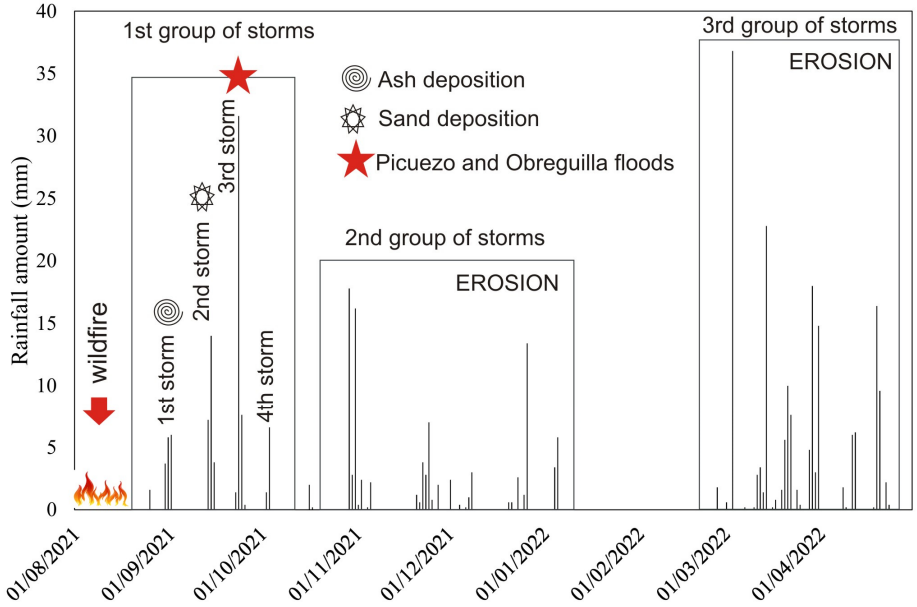


Figure 5. Rainfall events after the wildfire. Distribution of groups of storms (G1, G2, and G3) and relationships with ash, sand, and flood occurrence at the Avila rainfall station (2444).

The radar imagery shows a similar trend to the Avila rainfall station, with low precipitation in the study area. Despite having similar distributions, the total amounts differed between the radar and systematic gauging due to the convective nature of the storm.

The second group of storms, G2 (events 5 to 8), of low magnitude (occurring 2 to 4 months after the wildfire) and limited amounts of rainfall (~18 mm) revealed the beginning of the erosional processes in the burned area. The spring rains were the third group of storms, G3 (events 9 to 13), and, despite having moderate values (~36 mm), like those of the 23–24 September event, these rains did not involve new sediment mobilization in the burned area. Subsequently, during the hydrological year of 2022–2023, other moderate rains occurred, but the rivers' morphologies did not change, and the sediment remained stored in the sink areas.

A detailed survey of the radar images taken during the first group of events (G1, Table 1) confirmed the data from the Avila station and revealed that the rainfall duration of the first group of storms mostly did not exceed 3 h of continuous precipitation, except for the third storm of G1, which was divided into two consecutive storms of ~90 min separated by 4 h without rain, with a total cumulative precipitation of 63.8 mm/7 h. The average storm intensity ranged from 5 to 20 mm/h. The recurrence intervals for each event were lower than or equal to 2 years.

Table 1. Characteristics of every single event of the G1 group of storms: total rainfall, storm duration, and average storm intensity. Data are from radar imagery.

Storm Date	Total Storm Rainfall (mm)	Storm Duration (h:min)	Average Storm Intensity (mm/h)	Storm Recurrence (Years)
31 August 2021	29.4	2:20	12.6	<2
14 September 2021	13.2	1:00	13.2	<2
23/24 September 2021	27.6/34.2	1:30/1:40	18.4/20.52	2
29 October 2021	13.2	2:30	5.28	<2

4.2. Hydrological Changes

4.2.1. Water Repellency and Infiltration Changes

Water repellency was determined within the fire perimeter in adjacent unburned and burned soils (see sample locations in Figures 1, 3 and 6). Infiltration times were higher at most burned sites than at unburned sites. We observed differences depending on soil coverage. The predominant vegetation cover (>60%) in the study area is Mountain *Cytisus* formations. We measured infiltration in this cover at five of the nine sites (Figure 6d). Despite its lower fuel loadings in relation to its low biomass compared with a forest, the differences in infiltration between the burned and unburned areas were significant, by up to four times.

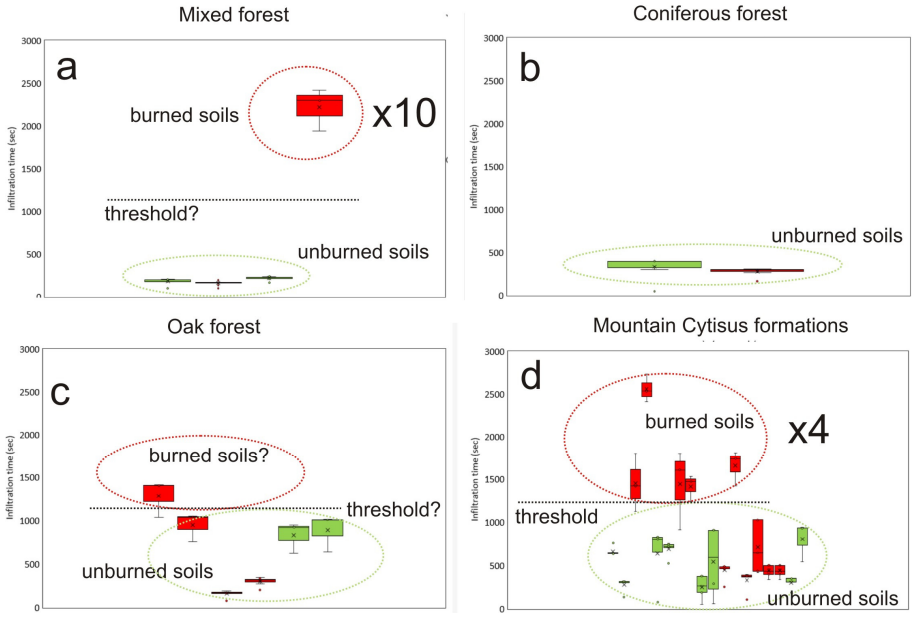


Figure 6. Infiltration rates in different soil coverages located within the wildfire perimeter. Red samples are burned soils and green samples are unburned soils.

In forested areas, such as mixed forest (Figure 6a), the differences between burned and unburned areas were higher (up to ten times); the dNBR map shows site 4 as having a moderate severity and a relatively high fuel content. However, the other forested areas, such as oak or pine forests (Figure 6b,c), revealed lower differences caused by post-fire management (machinery removed soil in the pine forest and, thus, increased infiltration). Unfortunately, we did not analyze the forest patches at the core of the wildfire due to the impossibility of comparison with nearby unburned areas.

Some samples showed similar infiltration times to those from areas with a low severity index.

We detected several differences in the results of the infiltration test due to the low degree of severity (low dNBR index), freeze–thaw cycles that waterproofed the soil during the sampling, and post-fire operational management.

Due to the homogeneous nature of the granitic soils in the studied area, we proposed a preliminary threshold for fire-induced water repellency, a factor that may contribute to a reduction in infiltration rates in unburned soils.

4.2.2. Hydrodynamic 2D Model

The Obreguilla Creek and Picuezo River basins show clear morphometric differences in terms of the total area, mean slope, river reach slope, and land cover. All these variables determine the hydrological behavior and the peak flows generated in the basins by storms.

Discharge hydrographs and shear stress values were used to assess the hydrodynamic behavior and changes in the Obreguilla Creek and Picuezo River basins due to the Navalacruz 2021 wildfire.

The discharge hydrographs of the Obreguilla Creek and Picuezo River basins (Figure 7) show differences. For Obreguilla Creek, the pre- and post-fire conditions were responsible for both a significant increase in the peak flow values under post-fire conditions and a time reduction in hydrograph peak flow generation. The peak flow values increased by more than 25% (from less than 4 m^3 s^{-1} to more than 5 m^3 s^{-1}), and their occurrence was 18 min early under post-fire conditions (from 00:05 h to 00:23 h of 1 September).

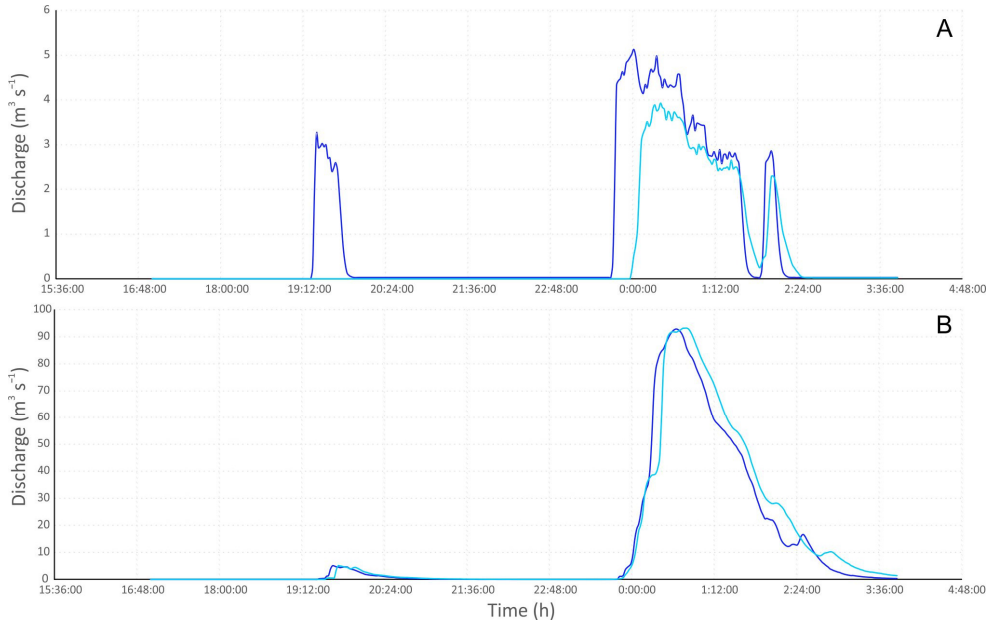


Figure 7. Discharge hydrographs for the (**A**) Obreguilla and (**B**) Picuezo basins under pre- and post-fire conditions (light and dark blue lines).

The previous clear differences between the pre- and post-fire results in Obreguilla Creek were not observed for the Picuezo River. Figure 7 shows very similar discharge hydrographs for the Picuezo River basin, with equal peak flow values (even slightly higher under pre-fire conditions; 93.24 m^3 s^{-1} and 92.88 m^3 s^{-1} for pre- and post-fire models, respectively) and peak flow times separated by only 7 min (from 00:39 h under post-fire conditions to 00:46 h of 1 September).

The shear stress results show similar trends to the discharge hydrographs, where hydrodynamic changes are more evident in the small basin of Obreguilla Creek. For this small-stepped basin, the ratio between the post- and pre-fire shear stress values shows a dominant increase in sediment transport capacity (Figure 8A). Despite the existence of localized areas with a high increase in sediment transport capacity (shear stress ratios higher than 3–4, as on both sides of the main channel defining the alluvial fan), most of the area shows an increase lower than 2 for the shear stress ratio.

The shear stress ratio between the post- and pre-fire conditions shows a more complex spatial distribution for the Picuezo River reach analyzed. A succession (Figure 8B) of areas with an increasing and decreasing sediment transport capacity was observed. The mean shear stress ratio for the area shows a slight increase in sediment transport capacity, which is more evident in the upstream area. However, when looking at the downstream reach of the Picuezo River (Figure 8B), the areas with an increasing sediment transport capacity are localized in the main channel, while the channel sides and floodplain predominantly show a decrease in the shear stress values.

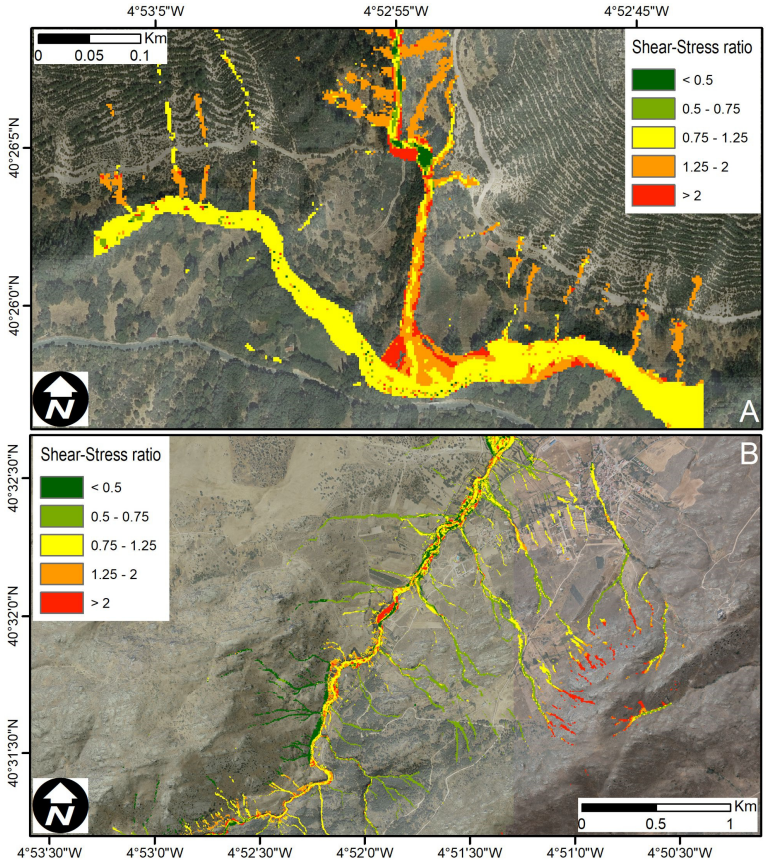


Figure 8. The shear stress ratio from hydrodynamic model results under pre- and post-fire conditions in the (**A**) Obreguilla and (**B**) Picuezo basins. The values of the ratio show the relationship between shear stress (τ) in post-fire and pre-fire conditions ($\tau_{\text{post-fire}}/\tau_{\text{pre-fire}}$).

The shear stress ratio results show differences between the Obreguilla and Picuezo basins, with Obreguilla showing a greater increase than the Picuezo basin. For Obreguilla Creek, the shear stress value under the post-fire conditions is 1.2–2-fold higher than that under the pre-fire conditions. These values are similar to the upper part of the Picuezo reach, where the shear stress ratio decreases to a mean value of 0.7–1.25-fold under the pre-fire conditions.

Thus, these results highlight a significant change in the hydrodynamic behavior of the small, circular, and stepped Obreguilla Creek basin (Figure 8A), where the post-Navalacruz 2021 wildfire conditions drove an increase in the peak discharge and potential sediment transport capacity (by increasing the shear stress). However, the results for the medium (although still less than 25 km^2), elongated, and less stepped Picuezo River basin do not show this clear significant change in hydrodynamic behavior. The peak flow values remain constant in magnitude and time scale, and the shear stress ratio does not show a homogeneous increasing trend in sediment transport capacity.

4.3. River Response

4.3.1. Changes in Morphology

We studied the morphological changes in the channels during the first year after the wildfire at 22 stations (see Figure 1). As the wildfire occurred at the end of summer, there was less than one month between the fire and the first rains. The main morphological effects are shown in Table 2. During the first group of events (1–4), mainly ash and flotsam entrainment occurred (events 1 and 2), followed by sediment mobilization, mainly sand from the regolith in less covered areas due to the wildfire. Most of the channels experienced aggradation, and sand bars covered the channels, leaving a drape-shaped

deposit with a continuous slope degree. This aggradation phase lasted until events 3–4, but it mostly occurred during event 2 and especially event 3. The greater amount of rainfall, together with the higher rainfall intensity, mobilized a large amount of sediment in the basins during event 3 (Figures 9 and 10). This event includes the flooding of the Picuezo River (24 September 2021), as well as the debris flow episode of Obreguilla Creek (Figure 8A). The high energy developed in this event could be observed in some channels, such as the Garganta de Toledo, where the entire sediment cover of a bedrock section was washed away, leaving a clean surface and bedrock erosion (Figure 9a). The mobilization of sands vs. coarser material in the debris depended on the specific spatial location of the moments of greatest intensity of the storm, as well as on the previous potential for the generation of sediment entrainment in each basin (slope and bedload availability). The Riofrío debris flow involved the blockage of a watercourse at the head of a knickpoint, with a change in the direction of the waterfall (Figure 9b). The degradation phase (incision) started during the second group of storms, events 5–10 (Figure 10). The sandbars with a regular slope angle became entrenched, and meandering embedded channels developed (Figure 10d,f). The channels widened in width, but erosion also reduced their height until they reached the original bed (Figure 10g). With the third group of storms, ~7 months after the wildfire, most of the fluvial network experienced a stabilization period (events 10 to 13). Remnants of sandbars and debris flows could be seen in protected areas of the floodplain. After the third group of storms, new rainfalls did not cause major changes in the river morphology. The longitudinal and cross-sectional profiles could be considered stable.

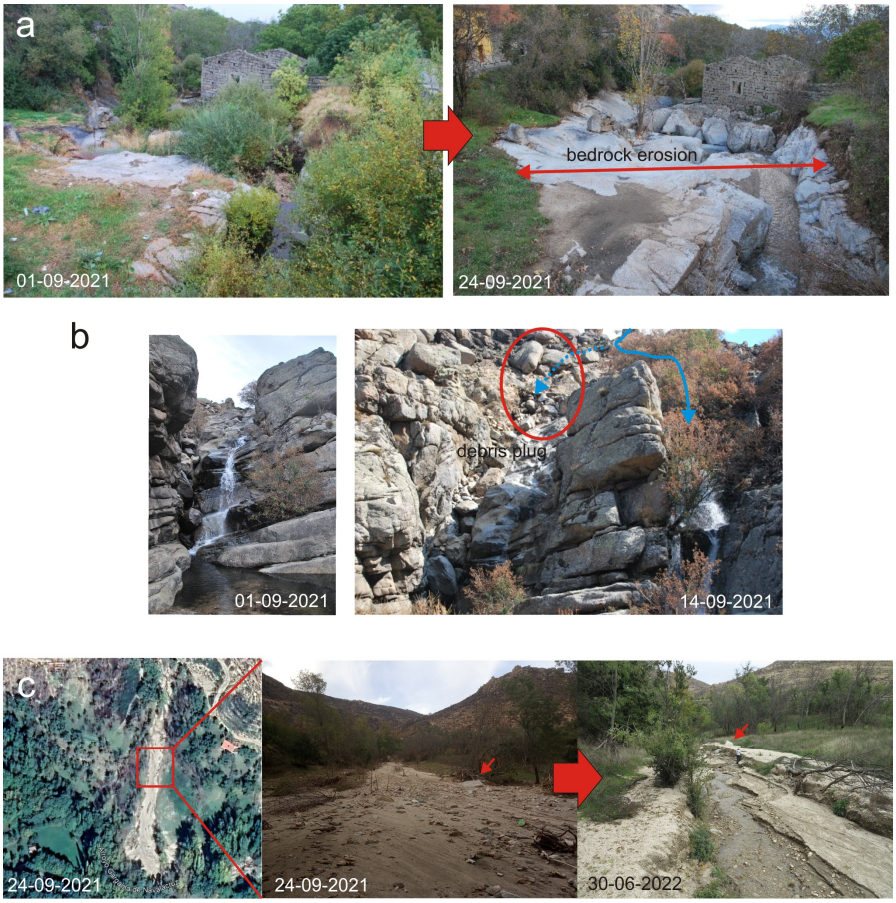


Figure 9. Morphological changes in bedrock reaches and debris flow generation. (**a**) Garganta de Toledo with low effects (ash deposition) of the 1st event (1 September 2021) vs. bedrock erosion of the 3rd storm (24 September 2021). (**b**) Riofrío stream, with a debris flow plug and change in waterfall course after the 2nd event. (**c**) Debris flow at Obreguilla Creek (24 September 2021) and subsequent erosion of deposits. Red arrows show the same point. Blue arrows show flow path.

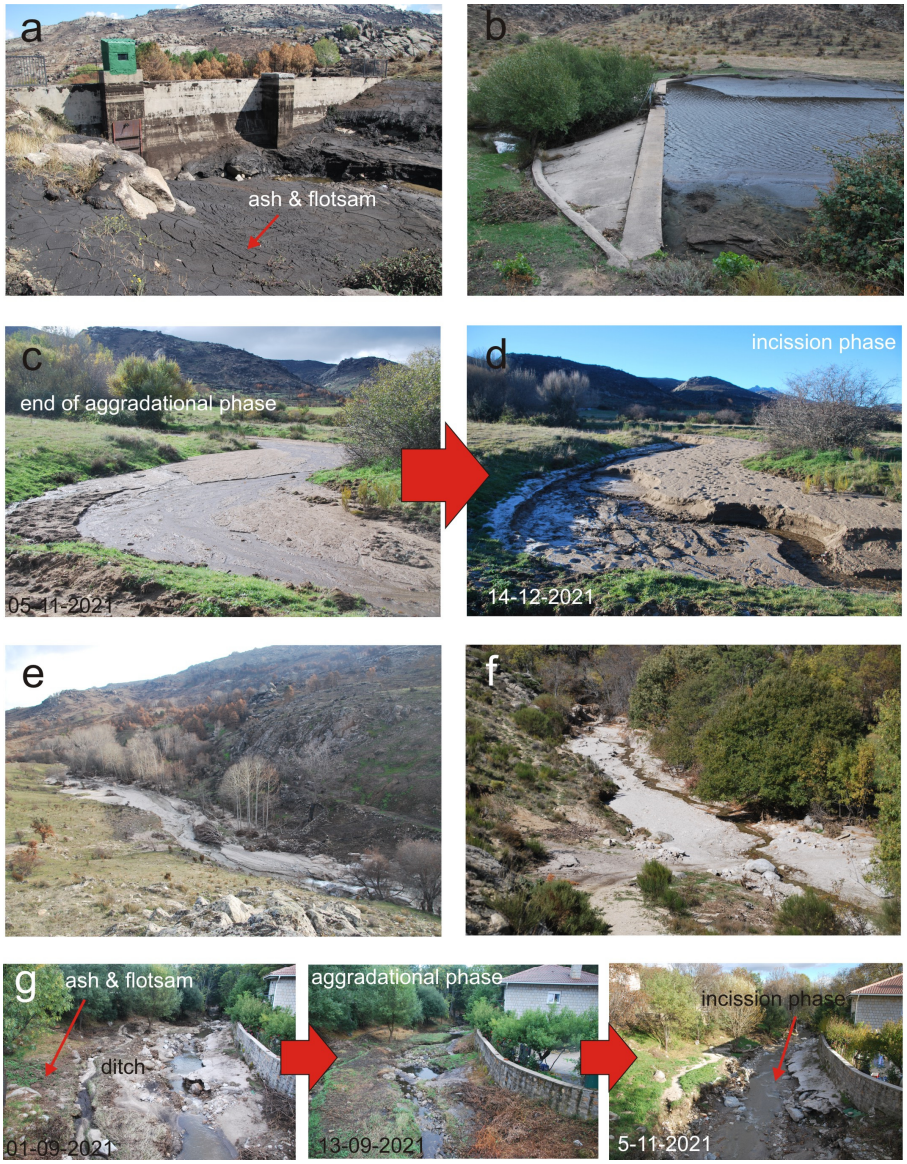


Figure 10. Morphological changes in alluvial reaches. (**a**) Dam filled with ash and silt during the 1st event in Garganta Honda. (**b**) Mironcillo check dam blockage during the 2nd event. (**c**) End of aggradational phase (photo taken on 5 November 2021) and (**d**) incision phase in Endrinal Creek. (**e**) Sand bars along the entire floodplain in the Picuezo River (photo taken on 19 December 2021). (**f**) Entrenched channel in sand bars in Garganta de Zapatero (photo taken on 28 October 2021). (**g**) Evolutionary sequence in Garganta de Zapatero, with ash and flotsam deposition during the first event, the aggradational phase, and finally the degradational phase before stabilization.

Table 2. Sequence of morphological changes in relation to the group of storms involved after the wildfire.

Morphological Changes	1st Storm Events (G1: 1 to 4)	2nd Storm Events (G2: 5 to 8)	3rd Storm Events (G3: 9 to 13)
Flotsam and ash deposition	Mostly in 1–2	–	–
Sand and mud bars	All, mostly in 2–3	–	–
Debris flows	Event 3	–	–
Bedrock exposed	Event 3	–	–
Post-flood erosion	–	Starts in 5	Decreases in 10
Stable	–	–	Starts in 10

We found five small dams in the burned area. Their use is mainly recreational, but there are also some dams for water supply and irrigation. All small dams were filled with sediment after the second event (Figure 10a,b).

4.3.2. Sediment Delivery to Mountain Streams

The combination of high slopes, above 40–45%, and the very high dNBR values (Figures 11 and S2) contributed to the high sedimentation rate in the study area. Within the two pilot basins, these characteristics, which drive sediment production, were related to the estimated sediment production values.

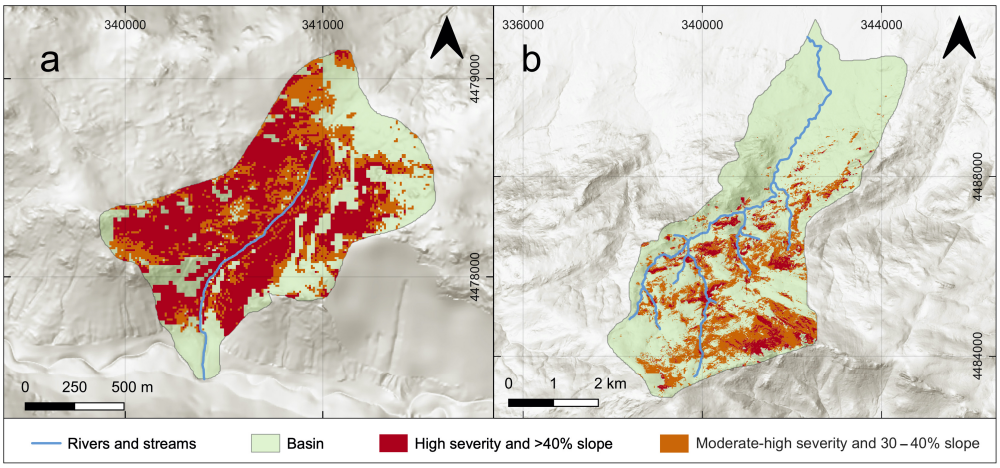


Figure 11. Susceptibility results in the two studied basins using the slope category and dNBR index: (**a**) Obreguilla basin, a small catchment facing southward with most of the basin area with 40–45% slopes and high dNBR values; (**b**) Picuezo basin, one of the larger catchments in the studied area, facing northward and with high slope and dNBR values in the upper basin.

Based on the results of the 2D hydrodynamic model and Equation (4), we estimated the change in the bedload transport capacity associated with the wildfire in both the Obreguilla and Picuezo Rivers. In the case of Obreguilla, we calculated a remarkable increase in the channel's capacity to transport bedload, i.e., an average ratio of 3.0 between the post-fire and pre-fire bedload capacities. In the case of the Picuezo River, the assessed change in bedload capacity was less marked: we estimated an average ratio of 1.1 between the post-fire and pre-fire bedload capacities. However, this result could be biased by the effect of assuming no change in the channel bed grain size. If we assumed that the fire was associated with an increase in fine material inputs to the channel and that the bed grain size was therefore refined (Dpre/Dpost = 2), then we would have estimated a post-/pre-ratio of 47.5 and 17.2 in the Obreguilla and Picuezo Rivers, respectively.

To obtain a quantitative volumetric estimate of bedload sediment delivery, a field survey was carried out to record the sediment thickness along the Obreguilla and Picuezo Rivers (Figure 12). The sediment thickness data were then used to derive a post-fire surface topography. Finally, the Geomorphic Change Detection (GCD; [57,58]) tool was used to compare the pre- and post-fire surface topographies. For Obreguilla Creek, the GCD analysis resulted in an estimated sediment volume of ~6400 m^3 of sediment, a value that takes into account sediment and pores. For this type of sediment, a porosity of about 35% is usually considered [59], so the sediment volume could be reduced to ~4200 m^3. For the Picuezo River, the first estimation, taking into account the sediment and the pores, gave a value of ~133,000 m^3, a result that could be reduced to ~99,800 m^3 if the volumetric porosity is not taken into account.

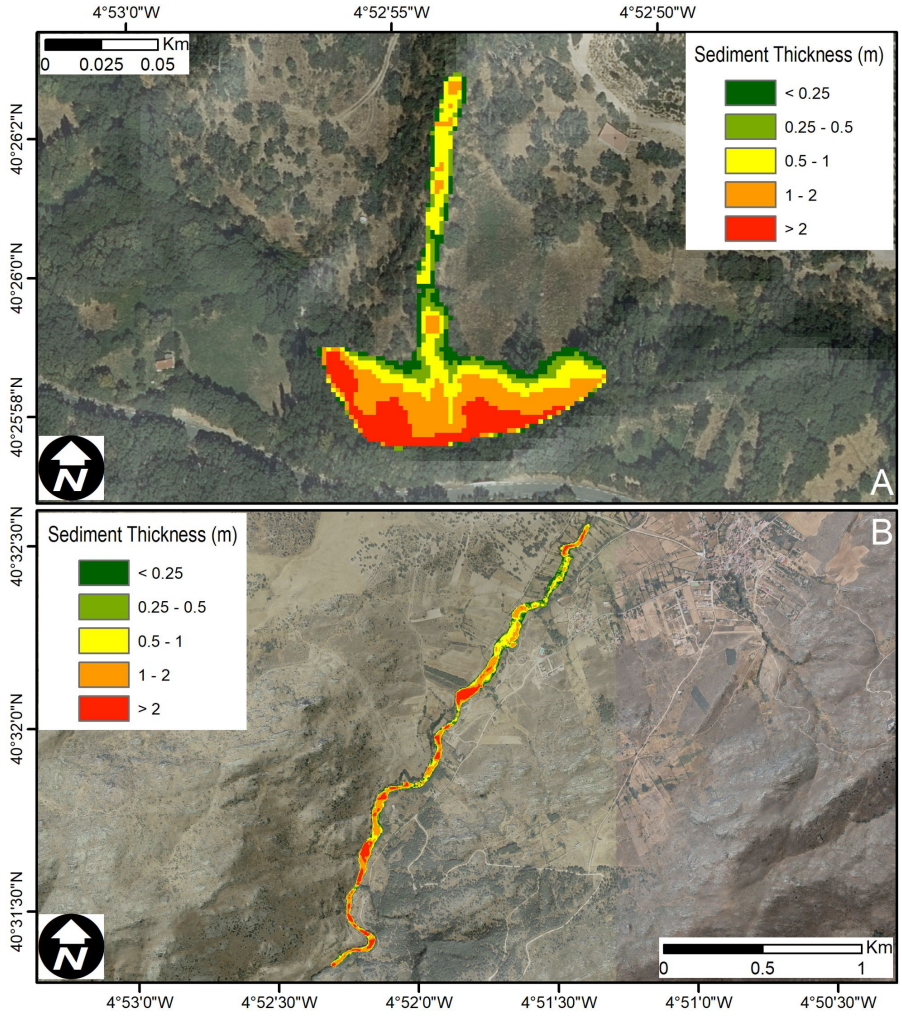


Figure 12. Sediment delivery in the two studied basins: (**A**) debris flow extent in the Obreguilla catchment and isopachs of sediment thickness; (**B**) medium Picuezo River.

We also estimated the amount of bedload remobilized during the 2021 post-fire storm using Equation (5). In the case of Obreguilla, we computed a bedload volume between 2300 and 4000 m^3, depending on the β coefficient used in Equation (5) (2 and 8, respectively). The calculated volumes were in the same order of magnitude as those obtained from topographic surveys in the field. In the case of the Picuezo River, the estimated volumes ranged between 8400 (β coefficient = 2) and 13,500 m^3 (β coefficient = 8). The assessed volumes were one order of magnitude lower than those derived from the topographic analysis. These differences may indicate that the volumes determined using the topographic analysis also included a large proportion of sediment transported as a suspended load, which was not adequately reproduced by bedload computation.

4.4. Effects on Cultural Heritage

The burned area constitutes an important heritage complex and is also part of the protected area Natura 2000 network ZEC "Sierra de la Paramera y Serrota". The most valuable cultural heritage structure of the area is the Celtic hillfort of Ulaca, one of the most interesting *oppidum* (Celtic fortified cities) in all of Europe of the Vetton culture (Iron Age). This type of structure is typical of the Iberian Peninsula, and some of the "castros" were used in the post-Roman period. Fortunately, although the archaeological site was surrounded by fire, it did not burn.

In the wildfire area, there are at least 60 cultural assets [29] (Figure 13), comprising archaeologically, ethnologically, and historically important sites, three of which are listed as

goods of cultural interest (BIC, the highest level of protection for cultural heritage in Spain). Most of them are related to the Vetton culture, but others are also valuable archaeological assets, such as the Roman road, necropolis, rock paintings, ancient hydraulic mills, the Visigothic village of Cabeza de Navasangil, and the medieval castle of Aunqueospese (Figure 14a). All of them are protected within the Spanish archaeological heritage laws.

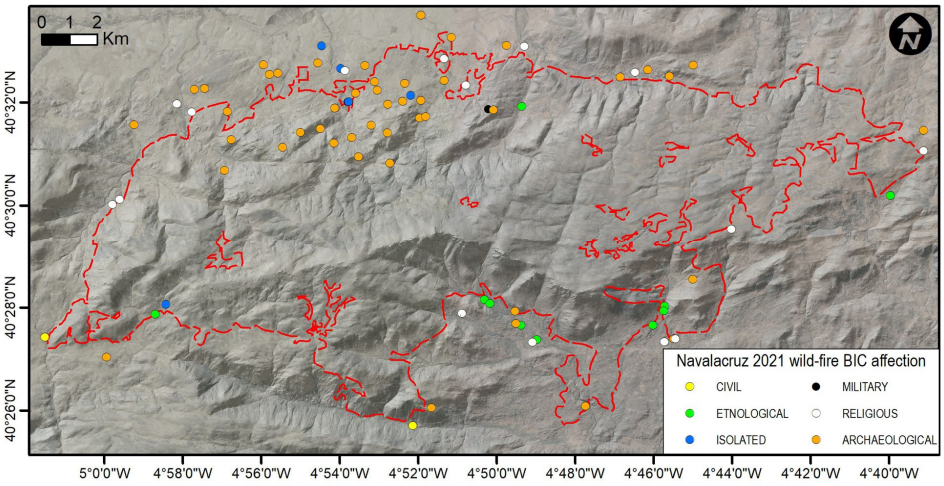


Figure 13. Cultural assets protected by Spanish laws (BICs) affected by the wildfire or subsequent flooding and divided into categories. The red dashed line shows the full perimeter of the Navalacruz 2021 wildfire.



Figure 14. Wildfire effects on cultural heritage. (**a**) Aunqueospese medieval castle in Mironcillo (XV century). (**b**) Vetton (Celtic) sacred stone called "Canto de los responsos". (**c**) Burned area of Visigothic village of La Cabeza de Navasangil. (**d**) Ancient mills covered by sandbars of the Picuezo River. (**e**) Quemado hydraulic mill, partially damaged and covered by sand bars. (**f**) Muñico historical bridge (1893), collapsed during the flood on 23 September. All pictures were taken after the wildfire.

Of all the cultural assets, the list of damage is the following [29]: nine did not suffer from any type of damage (level 0), forty cases had light damage (level 1), seven had moderate damage (level 2), three elements had serious damage due to a previous vulnerable situation or due to operational damage (level 3), and one ethnographic element had to be classified as a ruin/collapse (level 4).

Among the fire-damaged sites is the "Canto de los Responsos" (Figure 14b), an isolated boulder located 3 km SW of the Celtic oppidum of Ulaca (Ávila). It is associated with a Celtic folk ritual for travelers. Surrounded by scrubland and mountain pastures, it was affected by the fire but not destroyed; its dNBR index was moderate to low due to the low fuel content. The archaeological site of Cabeza de Navasangil (Figure 14c) was completely affected. This Visigoth village from the 5th century is composed of rock walls with partial damage to the ashlars (spalling).

However, one of the worst impacts on cultural heritage came from the high rainfall that resulted in soil erosion, affecting both the non-channeled phase of the slopes and all riverbeds of the fluvial network. Most of the cultural assets are sites scattered on the slopes, and many of these sites have been covered by deposits.

There is also a listed ethnological heritage site comprising numerous water mills that were covered or destroyed by post-fire floods, for example, the mills of the Picuezo River, comprising six hydraulic mills (Figure 14d), and the destruction of the Molino del Quemado (Figure 14e). The Muñico historic bridge, built in 1893, survived the fire, but it unfortunately collapsed just ten days later, damaged during the floods produced by the storm of 23–24 September. This bridge can be used as a marker of the return period of the event (the rainfall during that event did not exceed 2–3 years, and the bridge had 125 years of undamaged history (Figure 14f)).

5. Discussion and Conclusions

We observed intense runoff during the first events immediately after the fire, as suggested in [11,13,14]. The onset of stream sedimentation occurred early, during the first group of moderately sized storms (see Figure 5), consistent with the findings of Ref. [12]. The combination of the first post-fire floods with the first fall convective storms was the reason for the amount of sediment produced, as suggested by Ref. [16], accounting for 90% of it. However, this was not the only reason for the large amount of sediment. We observed a thick regolith in the weathering mantle limited by denudation on both the northern and southern sides of the burned area. This is consistent with the results of Ref. [34]. According to the above-mentioned authors, this indicates that slow weathering and deep infiltration led to the production of both a thick regolith and a wide reaction front.

Despite the low magnitude of rainfall events (~2 years), we reported some debris flow events associated with the previous high slope percentage >40% and the combination with the medium-to-high severity of the fire (see Figure 11). The rate of infiltration in deep weathered areas probably exceeded the rate of percolation, according to Ref. [60], causing the increase in pore pressure. Other events of this magnitude associated with small storms have been reported by Refs. [5,19], suggesting the triggering of debris flows with average intensities between 1 and 32 mm/h, and we found intensities of 20 mm/h. Conversely, Ref. [20] pointed out that return periods are greater than those of low magnitude, but these authors agree with >30% of slopes being particularly susceptible to soil erosion.

Morphological changes in fluvial systems rapidly occur in three stages: first, ash and flotsam deposits form; second, sand deposition and massive aggradation occurs during the following two months; and, third, erosional processes with channel entrenchment and lateral erosion occur up to 7 months after the wildfire. Our results are consistent with those of other morphological works, such as those by Ref. [3]. Within a few months after the wildfire, most of the streams stabilized, and a particular quantity of transient sediment had been mobilized, transported, and stored in the channels and floodplain.

Our results show medium rates of the severity index in the studied area (Figure 3). During the field infiltration test on the wildfire perimeter, we recorded clear differences

(×10 times) in the forested areas and Mountain *Cytisus* formations due to fuel availability that led to more hydrophobicity. However, the mountain pastures and other land coverages provided unclear results, probably because they are located on the wildfire perimeter under near fire extinction conditions.

A limitation of the present analysis was the paucity of available data on the pre-fire channel conditions. As a result, it was not easy to compare the post-fire and pre-fire channel response to previous seasonal periods of similar precipitation and to establish a robust conceptual cause–effect model of the influence of wildfire in the study streams. To overcome this shortcoming, we performed two analyses in the present study: (1) we measured soil infiltration in the field and compared soil infiltration in burned and unburned areas, and (2) we used hydrological–hydraulic modelling to compare pre- and post-fire hydraulic conditions (i.e., flow rates, shear stress) under a similar rainfall scenario.

Wildfires cause a loss of vegetation cover and a hydrophobic effect in the soil of burned areas. These processes were incorporated into the hydrodynamic model by changing the values of the SCS-CN and Manning's coefficient. The SCS-CN value increases under post-fire conditions, e.g., [47,61], due to the lower infiltration rates of burned soils and the lower interception of rainfall by vegetation cover; although conditioned by pre-fire SCS-CN values, the change between the pre- and post-fire conditions was lower than that indicated by Ref. [62]. The ratio of infiltration rates for burned and unburned sites in the Mediterranean mountains was 0.9, indicating relatively little change, but this ratio ranged from 0.3 to 0.5 for the sites in Spain [63,64]. Conversely, Manning's coefficient decreases when vegetation cover is burned or when pre-fire land cover is replaced by other types that are more representative of post-fire conditions. The reduction in Manning's coefficient has been estimated to be around 40% (e.g., [50,65]), although [65] shows reductions in Manning's coefficient of up to 56%. However, this reduction rate was highly dependent on the distribution and density of the pre-fire vegetation cover and could not be applied to rock outcrops with no vegetation or a very low density.

These changes in the pre- and post-fire conditions caused different hydrodynamic responses in the Obreguilla and Picuezo basins. The small and steep Obreguilla Creek basin showed some changes in its hydrological behavior, which could be summarized as a significant increase in peak flow, in agreement with Refs. [62,66,67]. At the same time, there was an increase in hydrological sensitivity, which is in agreement with Ref. [68], who reported that the rainfall thresholds for flow generation decreased after wildfires; this was evident when runoff was generated by the first rainfall under post-fire conditions, whereas no such runoff occurred under pre-fire conditions. However, other findings by Ref. [68], such as the absence of changes in peak flows or the duration shortening of flow events, were not observed here. The effect of the fire on the hydrological response is consistent with the conclusions of Ref. [69], who stated that smaller catchments are more sensitive to the effects of wildfire.

However, and as pointed out by Ref. [9], the hydro-sedimentary impacts on river basins vary according to the basin characteristics, such as size, climate, and, of course, pre- and post-fire conditions. These differences could be observed in the results for the Picuezo River, where neither peak flow nor hydrograph volume differed from the pre- to post-fire conditions. The hydrological behavior of the Picuezo River basin seems to be similar to that indicated by Ref. [67], who observed no difference in peak flow, but it is not consistent with their results of a faster response of flow to precipitation. The last point is a common process, as mentioned by Refs. [65,68,70], and it was an observable behavior in the Obreguilla basin but not in the Picuezo basin.

All of these hydrological changes are related, among other variables, to the sediment yield behavior of the catchment. From a hydrodynamics perspective, shear stress changes could control the bedload sediment transport capacity of the channel. The results of the Obreguilla and Picuezo Rivers showed an increase in the bedload sediment transport capacities resulting from the changes in shear stresses. This is in agreement with areas with extensive sediment deposits linked to post-fire rainfall events and high volumetric estima-

tions from a DEM of Difference (DoD) analysis. From the DoD analysis, the Obreguilla basin had a yield of about 26 t ha^{-1}, a really high value related to that recorded (19.7 t ha^{-1}) by Ref. [71] in the southeast of France. For the Picuezo basin, the same analysis showed a rate of about 46.5 t ha^{-1}, which is close to the highest value recorded by Ref. [67] and related to that recorded (0.017–50 t ha^{-1}) by Ref. [72] in southeastern Australia. All these values are still far from those reported by Ref. [6] from post-fire debris flows (113–294 t ha^{-1}).

Based on the field observations and hydrodynamic model results (with higher shear stress ratios within channels), it was determined that the main source of sediment in the Obreguilla and Picuezo basins could be channel erosion, as in the analysis by Refs. [73,74], rather than slope erosion, as in the analysis by Ref. [72]. However, our results show differences that may be related to basin characteristics and pre- and post-conditions, as well as possible differences in the fine sediment available for transport; the thickness; and the stony soil cover, which had a variable potential of available sediment for transport [9,68].

All these effects constitute a risk to cultural heritage sites in runoff areas and along water courses, which adds to the immediate breakdown effects that a fire itself may cause. Scattered archaeological sites located on slopes and water-related structures (water mills and bridges) are the cultural heritage assets that are more sensitive to the combined risk of fire and the subsequent sediment mobilization. In total, 85% of the inventoried cultural heritage sites in the area were affected to some extent by the fire, and 18% of them showed moderate-to-severe damage. Most of the severe damage caused to the heritage sites as a consequence of this fire event was due to sediment mobilization and flooding, which speaks to the relevance of this short-term destructive effect of wildfires on heritage sites.

Supplementary Materials: The following supporting information can be downloaded at: https://www.mdpi.com/article/10.3390/fire7020052/s1.

Author Contributions: Conceptualization, J.A.O.-B.; methodology, J.A.O.-B., J.G. and D.V.-T.; formal analysis, J.A.O.-B., J.G., M.G.-H. and D.V.-T.; investigation, all authors; field analysis, J.A.O.-B., C.S., J.G. and D.V.-T.; writing—original draft preparation, all authors; writing—review and editing, all authors; supervision, J.A.O.-B.; project administration, M.G.-H. All authors have read and agreed to the published version of the manuscript.

Funding: This research was funded by MCIN/AEI/10.13039/501100011033, grant numbers PID2020-116896RB-C21 and PID2020-116896RBC22, provided by MCIN/AEI/10.13039/501100011033.

Institutional Review Board Statement: Not applicable.

Informed Consent Statement: Not applicable.

Data Availability Statement: Data are available upon request by the corresponding author.

Acknowledgments: The authors would like to thank Cristina Escudero, for her support throughout this research. We also thank Jesus Abad for lending us the pictures of before and after the wildfire and Jose Vicente Albero (AEMET) for his valuable help with radar images. The authors acknowledge two anonymous reviews that improved the manuscript. C.S.'s fieldwork was partially funded by an UAM BSc Thesis fieldwork grant.

Conflicts of Interest: The authors declare no conflicts of interest.

References

1. Grenfell, M.C.; Abrahams, E.; Fisher, R.M. Analysis and conceptual geospatial modelling of the intermediary role of wetlands in drylands in post-fire material flux dynamics, Silvermine River catchment, Cape Town. *Wetl. Ecol. Manag.* **2022**, *30*, 623–645. [CrossRef]
2. Benda, L.; Miller, D.; Bigelow, P.; Andras, K. Effects of post-wildfire erosion on channel environments, Boise River, Idaho. *For. Ecol. Manag.* **2003**, *178*, 105–119. [CrossRef]
3. Eaton, B.C.; Andrews, C.A.E.; Giles, T.R.; Phillips, J.C. Wildfire, morphologic change and bed material transport at Fishtrap Creek, British Columbia. *Geomorphology* **2010**, *118*, 409–424. [CrossRef]
4. Shakesby, R.A.; Doerr, S.H. Wildfire as a hydrological and geomorphological agent. *Earth-Sci. Rev.* **2006**, *74*, 269–307. [CrossRef]
5. Cannon, S.H.; Gartner, J.E.; Wilson, R.C.; Bowers, J.C.; Laber, J.L. Storm rainfall conditions for floods and debris flows from recently burned areas in southwestern Colorado and southern California. *Geomorphology* **2008**, *96*, 250–269. [CrossRef]

6. Nyman, P.; Smith, H.G.; Sherwin, C.B.; Langhans, C.; Lane, P.N.J.; Sheridan, G.J. Predicting sediment delivery from debris flows after wildfire. *Geomorphology* **2015**, *250*, 173–186. [CrossRef]
7. Keller, E.A.; Valentine, D.W.; Gibbs, D.R. Hydrological response of small watersheds following the Southern California Painted Cave Fire of June 1990. *Hydrol. Process.* **1997**, *11*, 401–414. [CrossRef]
8. Ball, G.; Regier, P.; González-Pinzón, R.; Reale, J.; Van Horn, D. Wildfires increasingly impact western US fluvial networks. *Nat. Commun.* **2021**, *12*, 2484. [CrossRef] [PubMed]
9. Neary, D.G.; Ryan, K.C.; DeBano, L.F. (Eds.) *Wildland Fire in Ecosystems, Effects of Fire on Soil and Water*; General Technical Report RMRS-GTR-42; U.S. Department of Agriculture, Forest Service Rocky Mountain Research Station: Fort Collins, CO, USA, 2005; 250p.
10. Smith, H.G.; Sheridan, G.J.; Lane, P.N.J.; Bren, L.J. Wildfire and salvage harvesting effects on runoff generation and sediment exports from radiata pine and eucalypt forest catchments, southeastern Australia. *For. Ecol. Manag.* **2011**, *261*, 570–581. [CrossRef]
11. Cannon, S.H. Debris-flow generation from recently burned watersheds. *Environ. Eng. Geosci.* **2001**, *7*, 321–341. [CrossRef]
12. Kampft, S.K.; Brogan, D.J.; Schmeer, S.; MacDonald, L.H.; Nelson, P.A. How do geomorphic effects of rainfall vary with storm type and spatial scale in a post-fire landscape? *Geomorphology* **2016**, *273*, 39–51. [CrossRef]
13. Sillins, U.; Stone, M.; Emelko, M.B.; Bladon, K.D. Sediment production following severe wildfire and post-fire salvage logging in the Rocky Mountain headwaters of the Oldman River Basin, Alberta. *Catena* **2009**, *79*, 189–197. [CrossRef]
14. Wilson, C.; Kampf, S.K.; Wagenbrenner, J.W.; MacDonald, L.H. Rainfall thresholds for post-fire runoff and sediment delivery from plot to watershed scales. *For. Ecol. Manag.* **2018**, *430*, 346–356. [CrossRef]
15. DiBiase, R.A.; Lamb, M.P. Vegetation and wildfire controls on sediment yield in bedrock landscapes. *Geophys. Res. Lett.* **2013**, *40*, 1093–1097. [CrossRef]
16. Benavides-Solorio, J.D.; MacDonald, L.H. Measurement and prediction of post-fire erosion at the hillslope scale, Colorado Front Range. *Int. J. Wildland Fire* **2005**, *14*, 457–474. [CrossRef]
17. Ebel, B.A.; Moody, J.A.; Martin, D.A. Hydrologic conditions controlling runoff generation immediately after wildfire. *Water Resour. Res.* **2012**, *48*, 3529. [CrossRef]
18. Morán-Ordóñez, A.; Duane, A.; Gil-Tena, A.; De Cáceres, M.; Aquilué, N.; Guerra, C.A.; Brotons, L. Future impact of climate extremes in the Mediterranean: Soil erosion projections when fire and extreme rainfall meet. *Land Degrad. Dev.* **2020**, *31*, 3040–3054. [CrossRef]
19. Warrick, J.A.; Hatten, J.A.; Pasternack, G.B.; Gray, A.B.; Goni, M.A.; Wheatcroft, R.A. The effects of wildfire on the sediment yield of a coastal California watershed. *GSA Bull.* **2012**, *124*, 1130–1146. [CrossRef]
20. Gartner, J.E.; Cannon, S.H.; Santi, P.M.; Dewolfe, V.G. Empirical models to predict the volumes of debris flows generated by recently burned basins in the western US. *Geomorphology* **2008**, *96*, 339–354. [CrossRef]
21. Cannon, S.H.; Gartner, J.E.; Rupert, M.G.; Michael, J.A.; Staley, D.M.; Worstell, B.B. *Emergency Assessment of Postfire Debris-Flow Hazards for the 2009 Station Fire, San Gabriel Mountains, Southern California*; U.S. Geological Survey Open-File Report; U.S. Geological Survey: Reston, VA, USA, 2010; pp. 1–27.
22. Sanchez-Roda, A.; Oliva-Urcia, B.; Gomez-Heras, M. The Use of Magnetic Susceptibility as a Technique to Measure the Impact of Wildfires on Archaeological Heritage. *Appl. Sci.* **2022**, *12*, 10033. [CrossRef]
23. Yeste-Lizán, P.; Gomez-Heras, M.; García-Rodríguez, M.; Pérez-López, R.; Carcavilla, L.; Ortega-Becerril, J.A. Surface Mechanical Effects of Wildfires on Rocks in Climbing Areas. *Fire* **2023**, *6*, 46. [CrossRef]
24. Ryan, K.C.; Jones, A.T.; Koerner, C.L.; Lee, K.M. Wildland Fire in Ecosystems: Effects of Fire on Cultural Resources and Archaeology. In *Effects of Fire on Cultural Resources and Archaeology*; Department of Agriculture Forest Service, Rocky Mountain Research Station: Washington, DC, USA, 2012; Volume 3.
25. Gomez-Heras, M.; McCabe, S.; Smith, B.J.; Fort, R. Impacts of Fire on Stone-Built Heritage. *J. Archit. Conserv.* **2009**, *2*, 47–58. [CrossRef]
26. Vazquez, P.; Shushakova, V.; Gómez-Heras, M. Influence of mineralogy on granite decay induced by temperature increase: Experimental observations and stress simulation. *Eng. Geol.* **2015**, *189*, 58–67. [CrossRef]
27. Vazquez, P.; Benavente, D.; Montiel, D.; Gomez-Heras, M. Mineralogical Transformations in Granitoids during Heating at Fire-Related Temperatures. *Appl. Sci.* **2022**, *12*, 188. [CrossRef]
28. McCabe, S.; Smith, B.J.; Warke, P.A. Exploitation of Inherited Weakness in Fire-Damaged Building Sandstone: The "fatiguing" of "Shocked" Stone. *Eng. Geol.* **2010**, *115*, 217–225. [CrossRef]
29. Escudero, C. Forest fires and cultural heritage: Protection strategies in Castilla y León. *PROCULTHER-NET Project. Tech. Bull.* **2023**, *2*, 54–66. Available online: https://www.montesca.eu/proculther-net/PROCULTHER_NET_TECHNICAL_BULLETTIN_N2.pdf (accessed on 5 February 2024).
30. Palacios, D.; García, R.; Rubio, V.; Vigil, R. Debris flows in a weathered granitic massif: Sierra de Gredos, Spain. *Catena* **2003**, *51*, 115–140. [CrossRef]
31. Migon, P.; Thomas, M.F. Grus weathering mantles—Problems of interpretation. *Catena* **2002**, *49*, 5–24. [CrossRef]
32. Alejano, L.R.; Carranza-Torres, C. An empirical approach for estimating shear strength of decomposed granites in Galicia, Spain. *Eng. Geol.* **2011**, *120*, 91–102. [CrossRef]
33. White, A.F.; Blum, A.E. Effects of climate on chemical_ weathering in watersheds. *Geochim. Cosmochim. Acta* **1995**, *59*, 1729–1747. [CrossRef]

34. Bazilevskaya, E.; Lebedeva, M.; Pavich, M.; Rother, G.; Parkinson, D.Y.; Cole, D.; Brantley, S.L. Where fast weathering creates thin regolith and slow weathering creates thick regolith. *Earth Surf. Process. Landf.* **2013**, *38*, 847–858. [CrossRef]
35. Pavich, M.J. Processes and rates of saprolite production and erosion on a foliated granitic rock of the Virgina Piedmont. In *Rates of Chemical Weathering of Rocks and Minerals*; Colman, S.M., Dethier, D.P., Eds.; Academic Press: Orlando, FL, USA, 1986; pp. 551–590.
36. Olivé Davo, A. Mapa geológico de la hoja nº 555 (Navatalgordo). In *Mapa Geológico de España E 1:50.000 (MAGNA)*, 1st ed.; Instituto Geológico y Minero de España: Madrid, Spain, 2006; p. 75.
37. Martín Parra, L.M.; Matrínez-Salanova, J.; Moreno, F.; Contreras, E.; Iglesias, A.; Martín Herrero, D. Mapa geológico de la hoja nº 530 (Vadillo de la Sierra). In *Mapa Geológico de España E 1:50.000 (MAGNA)*, 1st ed.; Instituto Geológico y Minero de España: Madrid, Spain, 2006; p. 100.
38. EFFIS. European Union Forest Fire Report Informe n.º 123, 2022, European Commission. Available online: https://effis.jrc.ec.europa.eu/publications/bulletins-and-reports/ (accessed on 11 November 2023).
39. Keeley, J.E. Fire intensity, fire severity and burn severity: A brief review and suggested usage. *Int. J. Wildland Fire* **2009**, *18*, 116–126. [CrossRef]
40. USDA-ARS-NRCS. Soil Quality Test Kit Guide. Available online: http://www.nrcs.usda.gov/Internet/FSE_DOCUMENTS/stelprdb1044790.pdf (accessed on 20 October 2023).
41. Blade, E.; Cea, L.; Corestein, G.; Escolano, E.; Puertas, J.; Vázquez-Cendón, E.; Dolz, J.; Coll, A. Iber: Herramienta de simulación numérica del flujo en ríos. *Rev. Intern. Met. Num. Calc. Dis. Ingen.* **2014**, *30*, 1–10. [CrossRef]
42. U.S. Department of Agriculture (USDA); Natural Resources Conservation Service. National Engineering Handbook Hydrology Chapters; Chapters 4–10. Available online: https://directives.sc.egov.usda.gov/viewerFS.aspx?hid=21422 (accessed on 26 June 2023).
43. Boughton, W.C. A review of the USDA SCS Curve Number method. *Aust. J. Soil Res.* **1989**, *27*, 511–523. [CrossRef]
44. Ponce, V.M.; Hawkins, R.H. Runoff Curve Number: Has it reached maturity? *J. Hydrol. Eng.* **1996**, *1*, 11–19. [CrossRef]
45. Ministerio de Medio Ambiente y Medio Rural y Marino (MARM). *Guía Metodológica para el Desarrollo del Sistema Nacional de Cartografía de Zonas Inundables*; Ministerio de Medio Ambiente y Medio Rural y Marino: Madrid, Spain, 2011; pp. 289–294.
46. Higginson, B.; Jarnecke, J. *Salt Creek BAER-2007 Burned Area Emergency Response*; Hydrology Specialist Report; Unita National Forest: Prvo, UT, USA, 2007; 11p.
47. Kinoshita, A.M.; Hogue, T.S.; Napper, C. Evaluating Pre- and Post-Fire Peak Discharge Predictions across Western U.S. Watersheds. *J. Am. Water Resour. Assoc.* **2014**, *50*, 1540–1557. [CrossRef]
48. Chow, V.T. *Open-Channel Hydraulics*; McGraw-Hill Book Co.: New York, NY, USA, 1959; 680p.
49. Van Eck, C.M.; Nunes, J.P.; Vieira, D.C.S.; Keesstra, S.; Keizer, J.J. Physically-Based Modelling of the Post-Fire Runoff Response of a Forest Catchment in Central Portugal: Using Field versus Remote Sensing Based Estimates of Vegetation Recovery. *Land Degrad. Dev.* **2016**, *27*, 1535–1544. [CrossRef]
50. Wu, J.; Nunes, J.P.; Baartman, J.E.M.; Faúndez Urbina, C.A. Testing the impacts of wildfire on hydrological and sediment response using the OpenLISEM model. Part 1: Calibration and evaluation for a burned Mediterranean forest catchment. *Catena* **2021**, *207*, 105658. [CrossRef]
51. Recking, A. Simple method for calculating reach-averaged bedload transport. *J. Hydraul. Eng.* **2013**, *139*, 70–75. [CrossRef]
52. Recking, A.; Piton, G.; Vazquez-Tarrio, D.; Parker, G. Quantifying the Morphological Print of Bedload Transport. *Earth Surf. Process. Landf.* **2016**, *41*, 809–822. [CrossRef]
53. Recking, A.; Vázquez Tarrío, D.; Piton, G. The contribution of grain sorting to the dynamics of the bedload active layer. *Earth Surf. Process. Landf.* **2023**, *48*, 979–996. [CrossRef]
54. Rickenmann, D.; Koschni, A. Sediment loads due to fluvial transport and debris flows during the 2005 flood events in Switzerland. *Hydrol. Process.* **2010**, *24*, 993–1007. [CrossRef]
55. Shtober-Zisu, N.; Tessler, N.; Tsatskin, A.; Greenbaum, N. Accelerated weathering of carbonate rocks following the 2010 wildfire on Mount Carmel, Israel. *Int. J. Wildland Fire* **2015**, *24*, 1154–1167. [CrossRef]
56. Dorn, R.I. Boulder weathering and erosion associated with a wildfire, Sierra Ancha Mountains, Arizona. *Geomorphology* **2003**, *55*, 155–171. [CrossRef]
57. GCD. Geomorphic Change Detection Software. Version 7.5. 2015. Available online: https://gcd.riverscapes.net/Download/ (accessed on 5 September 2023).
58. Wheaton, J.M.; Brasington, J.; Darby, S.E.; Sear, D.A. Accounting for uncertainty in DEMs from repeat topographic surveys: Improved sediment budgets. *Earth Surf. Process. Landf.* **2010**, *35*, 136–156. [CrossRef]
59. Frings, R.M.; Schüttrumpf, H.; Vollmer, S. Verification of porosity predictors for fluvial sand-gravel deposits. *Water Resour. Res.* **2011**, *47*, W07525. [CrossRef]
60. Costa, J.E. Physical geomorphology of debris flows. In *Developments and Applications of Geomorphology*; Springer: Berlin/Heidelberg, Germany, 1984; pp. 268–317.
61. Papathanasiou, C.; Makropoulos, C.; Mimikou, M. Hydrological modelling for flood forecasting: Calibrating the post-fire initial conditions. *J. Hydrol.* **2015**, *529*, 1838–1850. [CrossRef]
62. Soulis, K.X. Estimation of SCS Curve Number variation following forest fires. *Hydrol. Sci. J.* **2018**, *63*, 1332–1346. [CrossRef]
63. Martin, D.A.; Moody, J.A. Comparison of soil infiltration rates in burned and unburned mountainous watersheds. *Hydrol. Process* **2001**, *15*, 2893–2903. [CrossRef]

64. De Imeson, A.C.; Verstraten, J.M.; Van Mulligen, E.J.; Sevink, J. The effects of fire and water repellency on infiltration and runoff under Mediterranean type forest. *Catena* **1992**, *19*, 345–361. [CrossRef]
65. Stoof, C.R.; Ferreira, A.J.D.; Mol, W.; Van den Berg, J.; De Kort, A.; Drooger, S.; Slingerland, E.C.; Mansholt, A.U.; Ferreira, C.S.S.; Ritsema, C.J. Soil surface changes increase runoff and erosion risk after a low–moderate severity fire. *Geoderma* **2015**, *239–240*, 58–67. [CrossRef]
66. Walsh, R.P.D.; Boakes, D.J.; Coelho, C.d.O.A.; Ferreira, A.D.; Shakesby, R.A.; Thomas, A.D. Post-fire land use management and runoff responses to rainstorms in Portugal. In *Geomorphology and Land Management in a Changing Environment*; McGregor, D.F.M., Thompson, D., Eds.; Wiley: Chichester, UK, 1995; pp. 283–308.
67. Ohana-Levi, N.; Givati, A.; Paz-Kagan, T.; Karnieli, A. Forest composition effect on wildfire pattern and run-off regime in a Mediterranean watershed. *Ecohydrology* **2018**, *11*, e1936. [CrossRef]
68. Greenbaum, N.; Wittenberg, L.; Malkinson, D.; Inbar, M. Hydrological and sedimentological changes following the 2010-forest fire in the Nahal Oren Basin, Mt. Carmel Israel–a comparison to pre-fire natural rates. *Catena* **2021**, *196*, 104891. [CrossRef]
69. Versini, P.A.; Velasco, M.; Cabello, A.; Sempere-Torres, D. Hydrological impact of forest fires and climate change in a Mediterranean basin. *Nat. Hazards* **2013**, *66*, 609–628. [CrossRef]
70. Candela, A.; Aronica, G.; Santoro, M. Effects of forest fires on flood curves in a Mediterranean catchment. *Hydrol. Sci. J.* **2005**, *50*, 193–206. [CrossRef]
71. Martin, C.; Allee, P.; Kuzucuoglu, C.; Levant, M. Mesure de l'erosion mechanique des sols apres un incendie de foret dans le massif des Maures. *Geomorph. Relief. Proc. Environ.* **1997**, *2*, 133–142. [CrossRef]
72. Smith, H.G.; Sheridan, G.J.; Lane, P.N.J.; Noske, P.J.; Heijnis, H. Changes to sediment sources following wildfire in a forested upland catchment, southeastern Australia. *Hydrol. Proc.* **2011**, *25*, 2878–2889. [CrossRef]
73. Moody, J.A.; Martin, D.A. Post-fire, rainfall intensity-peak discharge relations for three mountainous watersheds in the western USA. *Hydrol. Proc.* **2001**, *15*, 2981–2993. [CrossRef]
74. Moody, J.A.; Martin, D.A. Synthesis of sediment yields after wildland fire in different rainfall regimes in the western United States. *Int. J. Wildland Fire* **2009**, *18*, 96–115. [CrossRef]

Disclaimer/Publisher's Note: The statements, opinions and data contained in all publications are solely those of the individual author(s) and contributor(s) and not of MDPI and/or the editor(s). MDPI and/or the editor(s) disclaim responsibility for any injury to people or property resulting from any ideas, methods, instructions or products referred to in the content.